Journal Pre-proof

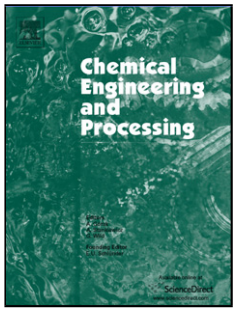

Process intensification through the use of multifunctional reactors for PEMFC grade hydrogen production: Process design and simulation

Izurieta Eduardo M., Adrover M. Esperanza, Pedernera Marisa N., López Eduardo

PII: S0255-2701(19)31232-2

DOI: https://doi.org/10.1016/j.cep.2019.107711

Reference: CEP 107711

To appear in: *Chemical Engineering and Processing - Process Intensification*

Received Date: 1 October 2019

Revised Date: 24 October 2019

Accepted Date: 31 October 2019

Please cite this article as: Izurieta EM, Adrover ME, Pedernera MN, Eduardo L, Process intensification through the use of multifunctional reactors for PEMFC grade hydrogen production: Process design and simulation, *Chemical Engineering and Processing - Process Intensification* (2019), doi: https://doi.org/10.1016/j.cep.2019.107711

Process intensification through the use of multifunctional reactors for PEMFC grade hydrogen production: Process design and simulation

Izurieta, Eduardo M.[1,2*] eizurieta@plapiqui.edu.ar , Adrover, M. Esperanza[1,2], Pedernera, Marisa N.[1,2], López, Eduardo[2]

[1]Departamento de Ingeniería Química, Universidad Nacional del Sur (UNS), Avenida Alem 1253, CP8000, Bahía Blanca, Argentina.

[2]Planta Piloto de Ingeniería Química – PLAPIQUI (Universidad Nacional del Sur – CONICET), Camino La Carrindanga km 7, CP8000, Bahía Blanca, Argentina.

*Corresponding Author.

Graphical abstract

Highlights

- A highly integrated process for electrical and heating power supply is studied.
- Ethanol steam reforming for H_2 production and subsequent purification is proposed.
- Parallel-plate reactors are implemented for achieving a highly intensified process.
- Membrane reactor is implemented for PEM fuel cell-grade hydrogen production.

Abstract

A highly integrated process aiming electrical and heating power supply is proposed. Ethanol, water and air at atmospheric conditions are considered as feedstocks. Main focus is put in process intensification through the use of parallel-plate and membrane reactors allowing the combination of different process operations within the units. The electric power is generated by means of a PEM fuel cell, which is fed with pure hydrogen produced by ethanol steam reforming with subsequent purification. Appropriate thermal integration is achieved both in the parallel-plate units as well as in the membrane reactor. The high temperature of the streams exiting the reformer allows preheating the air to the combustion sections and the sweep gas to the membrane reactor improving the process

integration and achieving an electrical production of 2.5 kW. In addition, a hot water stream is used to produce the cogeneration heat, increasing the total thermal efficiency up to 56.3%.

Keywords: Structured reactors; Process intensification; Hydrogen production; Ethanol steam reforming; Energetic integration

Nomenclature

A_{TM}	total cross-sectional area of flow in the membrane reactor	m^2
A_{TR}	total cross-sectional area of flow in the parallel-plate units	m^2
A_{TW}	total cross-sectional area of the metallic walls in the parallel-plate units	m^2
C_P	heat capacity of a stream	J/(mol·K)
d_t	diameter of the membrane tubes	m
Ea_M	activation energy of the permeation process	J/mol
E_{rev}	PEM fuel cell reversible voltage	V
Ex	total exergy of a stream	W
ex	molar exergy of a stream	J/mol
F	molar flowrate	mol/s
$\mathcal{F}$	Faraday's constant	C/mol
ΔH	heat of reaction	J/mol
H	molar enthalpy of a stream	J/mol
h	heat transfer coefficient	$W/(m^2 \cdot K)$
I_{PEM}	PEM fuel cell electric current	A
J_{H_2}	hydrogen permeation flux in the membrane reactor	$mol/(m^2 \cdot s)$

k_g	mass transport coefficient	m/s
L_W	thickness of the metallic wall in the parallel-plate units	m
L_X	width of the catalytic channels in the parallel-plate reactors	m
L_Z	length of the reactor	m
LHV	lower heating value	J/mol
$\dot{m}$	specific mass flowrate	kg/(m^2·s)
M	molecular weight	kg/mol
P	absolute pressure	bar
p	partial pressure of a species	bar
p^{sat}	saturation pressure	bar
Q_0	preexponential constant for the hydrogen permeation in the membrane reactor	mol/(m·s·atm$^{0.5}$)
Q_{co}	cogeneration heat	W
q_{lost}	heat loss to the environment at each axial coordinate in a unit	W/m
Q_{lost}	total heat loss to the environment by a unit	W
Q_{PEM}	refrigeration heat in the PEM fuel cell	W
q_w	heat transferred through the metallic wall in the parallel-plate units	W/m^2
R	universal gas constant	J/(mol·K)
r	rate of reactions in the parallel-plate reactors	mol/(m^2·s)
r_{CO}	rate of reactions in the membrane reactor	mol/(g·s)
R_{H_2}	percentual hydrogen recuperation in the membrane reactor	%
S	molar entropy of a stream	J/(mol·K)

T	temperature of a stream	°C or K
T^c	temperature of the catalytic phase in the parallel-plate reactors	°C or K
T_w	temperature of the metallic wall in the parallel-plate units	°C or K
U_M	global heat transfer coefficient in the membrane reactor	W/(m^2·K)
V_{PEM}	PEM fuel cell voltage	V
W_{PEM}	PEM fuel cell power	W
w_i	mass fraction of the species in the gas phase of the parallel-plate reactors	-
w_i^c	mass fraction of the species at the catalyst in the parallel-plate reactors	-
$X_{C_2H_5OH}^{RHX2}$	ethanol conversión in the RHX2 unit	%
X_{CO}^{MR}	carbon monoxide conversion in the membrane reactor	%
$X_{H_2}^{PEM}$	hydrogen conversion in the PEM fuel cell's anode	%
$X_{O_2}^{PEM}$	oxygen conversion in the PEM fuel cell's cathode	%
x_R	transversal coordinate of the metallic wall in the parallel-plate units	m
y	molar fraction	-
z_R	axial coordinate of the reactors	m
δ_M	thickness of the permeation layer in the membrane reactor	m
ε	standard chemical exergy	J/mol
η	thermal efficiency, see Eqs. 64 to 67	%
λ	thermal conductivity	W/(m·K)
ν	stoichiometric coefficient in a reaction	-
ρ	gas phase density	kg/m^3

ρ_B	catalytic bed density in the membrane reactor	kg/m^3
σ	total perimeter of the channels in the catalytic monolith	m
σ_M	total perimeter of permeation in the membrane reactor	m
σ_w	total perimeter of heat exchange with the metallic walls in the parallel-plate units	m
φ	PEM fuel cell overpotential	V

Subscripts

an	fuel cell's anode
cat	fuel cell's cathode
cs	cold-side stream in the parallel-plate units
hs	hot-side stream in the parallel-plate units
liq	liquid stream of the separation chamber
off	off-gas stream
per	permeate stream of the membrane reactor
ret	retentate stream of the membrane reactor
vap	vapour stream of the separation chamber

1. Introduction

The basic conditions for heat recovery and the minimization of energy losses in a process can be set through an exhaustive analysis of the overall energy balance of the system under study [1,2]. It has been found that it is possible to save large amounts of energy by analysing the problem from the context of the whole process by means of global integration techniques, instead of trying to optimize each unit separately [3]. On the other hand, process intensification (PI) arises from the need to minimize equipment size and the use of resources, simultaneously with the maximization of performance and

efficiency of these processes [4]. PI is a limit case of high integration with great advantages over traditional processes [5].

Process intensification and the development of new applications require a significant improvement in the design and performance of the reaction units. Multifunctional reactors are seen as an interesting alternative to achieve the PI through the integration of the chemical reaction with other types of unit operations in a single unit [6]. Structured and membrane reactors are both promising alternatives for achieving multifunctionality in chemical reactors.

Structured catalytic reactors comprising parallel channels with heat exchange between contiguous sections offer high area/volume ratios and very high heat transfer coefficients [7] achieving compact units with an efficient heat transfer/reaction integration. In addition, the modular nature of these designs makes the reactor scaling-up particularly simple. In these reactors, the fluid circulates through channels of defined geometry and the catalyst is generally deposited on structures arranged within the channels or directly on the wall of those channels. These designs present several advantages over conventional fixed-bed reactors as they operate with lower pressure drop and enhanced heat transfer rates through the walls is achieved.

Aiming reaction/heat transfer intensification, the heat exchanger reactors were developed for their application to highly exothermic or endothermic gas phase reactions [8]. In these designs, on one side of the compact exchanger the catalytic material is arranged by means of washcoating or by incorporating catalytic elements (pellets or structured packing). The service fluid circulates on the other side of the unit and either catalytic or inert structures can also be arranged to facilitate mixing and promote heat transfer conditions. As a result of this integration, not only more compact equipment is obtained but also a better control of the temperature, which could result in a safer operation and improvements in the selectivity and performance towards the desired product [9].

Particularly, the parallel plate reactors, in which a repetition of plates (usually metallic) separates sections of the reactor where different fluids circulate, can be applied to perform the thermal coupling of endo- and exothermic reactions in neighbouring sections [10]. The heat generated by the exothermic reaction is easily transferred to the endothermic one through a thin metallic wall. The direction of the flow through the different sections can also be selected with simplicity in co- or countercurrent, or in

cross flow, as appropriate. Furthermore, the geometric design of this reactor concept greatly simplifies the implementation of lateral feeds, sampling probes or measurement devices [11,12].

On the other hand, membrane reactors are units that allow combining the catalytic effect given by the catalyst and the separation effect provided by the membrane. The integration of these types of units offers advantages not only in terms of simplification of the equipment, but also introduces improvements in the selectivity and the yield of the reactor [13], impacting on the performance of the global process in which they are inserted, either through the permeation and purification of a specific product [14] or with the controlled addition of a reagent through the membrane [15,16].

Processes aiming power generation employing fuel cells at low scale for both mobile or decentralized facilities appear as interesting cases to apply the above-mentioned PI concepts. Fuel cells are highly efficient devices in which chemical energy is transformed into electrical energy, eliminating the process of fuel burning, thus improving energy yields by trespassing the restrictions imposed by the Carnot cycle. These devices suppose very low levels of associated pollution. In addition, they can be easily adapted to different requirements due to their modular characteristics.

The direct use of hydrogen is clearly the preferred choice towards fuel cells feeding. However, the absence of a H_2 distribution network and the risks and technological difficulties associated with its storage and transport have constrained the widespread implementation of this direct strategy. As an alternative, the successful implementation of the fuel cells in the short term can be conducted through the processing of liquid fuels by reforming them in situ. Among the different types of fuel cells, the proton-exchange membrane fuel cells (PEMFC) predominate in the generation of power at small scales such as the cases of residential units and for mobile applications due to the low temperature of operation, cheaper materials in its manufacture and faster start-up procedures. Although PEMFCs work ideally with a pure hydrogen feed, they are able of processing gas mixtures rich in H_2 with a slight decrease in their performance. However, it must be observed that PEMFCs use platinum as the anode electrocatalyst which is easily poisoned at low temperatures by carbon monoxide (reversibly) or by sulphur (irreversibly), among others. If the hydrogen-rich gas fed to the cell comes from reforming processes, it must be free of these polluting species.

Ethanol is an interesting source for the production of hydrogen because of its high H/C ratio, very low toxicity, easy transport and high energy density [17]. It is produced with a high amount of water that should not be removed as in the case of its use for internal combustion engines. Furthermore, bioethanol can be obtained from renewable resources (biomass and organic waste). First-generation bioethanol is obtained by fermentation of cereals, sugarcane or beet, among others in an industrial process established decades ago [18,19]. Second-generation bioethanol can be obtained from lignocellulosic biomass or also from the so-called energy crops (not suitable for food and generally grown on marginal lands, unsuitable for other purposes). In addition, bioethanol steam reforming would imply an almost closed cycle of carbon dioxide since the CO_2 generated by the reforming balances that previously consumed along the biomass growth [20]. In this way, its introduction as an energy vector could reduce the current emissions of CO_2 by up to 30% [21].

The catalytic reforming of ethanol with steam is globally represented by the following equation:

$$C_2H_5OH + 3\ H_2O \leftrightarrow 2\ CO_2 + 6\ H_2 \qquad \Delta H° = 173.4\ kJ/mol \qquad (1)$$

The overall reaction indicates a maximum production of 6 moles of H_2 per mole of ethanol fed. Despite this simple equation represents the global process, a complicated network of different reaction pathways leading to various end products and/or intermediates have been observed, depending on the type of catalyst used and the operating conditions [22]. Many of the intermediate reactions are limited by the chemical equilibrium imposing strong restrictions on the maximum hydrogen yield. Moreover, the high global endothermicity of the process implies the operation at high temperatures. This fact determines the need to achieve a high heat transfer fluxes to the reformer to avoid prohibitive losses in thermal efficiency, a challenging task in small-scale systems.

Previous studies demonstrated that parallel plate reactors proved an appropriate design to fulfil the thermal requirements imposed by the ethanol steam reforming reaction [23,24]. Satisfactory performances were achieved due to the high heat transfer rates between sections, in addition to the flexibility towards the coupling of endo- and exothermic reactions. To boost the heat transfer rates, different authors have reported the use of structured catalysts with high thermal conductivity in these type of reactor designs [25–28]. They state that these catalytic structures appear appealing in energy-intensive processes enhancing axial heat transport and thus diminishing the magnitude of hot spots.

The synthesis gas exiting the reforming reactor has considerable amounts of CO, which must be extensively reduced to be suitable to feed a fuel cell (e.g., up to ca. 10 ppm for PEMFCs). Hydrogen purification (i.e., CO removal) is usually carried out downstream the reformer, including water gas shift reactors, methanation, preferential oxidation of CO or PSA.

Seeking PI, the above-mentioned water gas shift (WGS) reaction can be implemented into a membrane reactor unit. Here, a H_2 stream of very high purity can be obtained satisfying the requirements for fuel cell feeding. In addition, this system overcomes the thermodynamic limitations by displacement of the chemical equilibrium, improving the hydrogen yield of the process [29].

This paper focus on the analysis of an intensified process aiming the generation of 2.5 kW of electric power with a H_2-fueled PEMFC. Ethanol, water and air are the intended feedstocks of the studied system. The proposed flow diagram of the process includes structured and membrane reactors to study how the intensification provided by these units impact over the overall performance. First and second-law efficiencies are evaluated in order to quantify the performance of the system and compare with data reported in literature.

2. Theoretical framework and mathematical model

2.1 Process description

Ultrapure hydrogen production from ethanol steam reforming is studied within the process described below. Figure 1 presents the flow diagram for the proposed process. The implementation of three structured catalytic reactors of the parallel-plates type is distinguished here (RHX units). These structured reactors are introduced to couple chemical reaction and heat exchanging in the same unit. A co-current configuration has been selected in all cases. The first reactor (RHX1) operates as a heat exchanger carrying out the evaporation and overheating of the reactive mixture (ethanol + water, stream 1) at expenses of the heat delivered by the catalytic combustion of the retentate stream leaving the membrane reactor, (MR, stream 5). Extra ethanol supply (stream 7) is planned as well. The combustion air (stream 15) enters through the main inlet of the RHX1 while the fuel streams are incorporated in different lateral injection ports (streams 8a to 8f) in order to obtain an adequate control

over the combustion reaction [23]. In the second parallel-plate reactor (RHX2), the ethanol steam reforming reaction proceeds, thermally coupled with the catalytic combustion of the fuel.

The structured reactor RHX3 aims the preheating of the combustion air stream to feed the RHX1. To this end, the unconsumed hydrogen exiting the fuel cell (stream 19) is catalytically burned in this unit. Simultaneously, the process stream leaving the RHX2 (i.e., syn-gas, stream 3) is cooled in the alternated sections of the reactor. The reduction in the thermal level of the syn-gas stream in RHX3 aims to conditioning the inlet to the MR to prevent catalyst sintering (T_{max} of 550 °C for the considered WGS catalyst).

All three parallel-plate reactors (RHX1-3) were thought to operate with a Pd/Al_2O_3 catalyst (0.5% Pd, Engelhard, commercial oxidation catalyst) since, according to previous works, this catalytic formulation presents appropriate activity/selectivity for both ethanol steam reforming [30] and combustion reactions [31,32]. This catalyst selection, i.e., the same catalyst for the different reactions involved, favours the simplicity of the process design.

The unit HX is designed as a non-catalytic countercurrent parallel-plate heat exchanger. This unit is intended to evaporate and overheat a water stream (stream 28) to be used as sweep gas in the membrane reactor. To this end, heat is transferred from the outlet stream of RHX2 (combustion side, stream 10).

As mentioned before, the purification sector comprises of a membrane multitubular reactor (MR) in which the WGS reaction takes place by means of a Fe/Cr/Cu catalyst:

$$CO + H_2O \leftrightarrow CO_2 + H_2 \qquad \Delta H° = -41.2 \text{ kJ/mol} \qquad (2)$$

The cooled synthesis gas that leaves the RHX3 flows through the shell of the MR, which is packed with WGS catalytic pellets. The tubes of the reactor are functionalized with a Pd membrane to selectively permeate the H_2 (with infinite selectivity). Water steam flowing through the tubes is selected as sweep gas in order to diminish the hydrogen partial pressure in the tubes and, consequently, enhance the permeation flux.

The permeate from the MR (hydrogen and water steam, stream 17) is cooled down to the PEMFC temperature in the separation chamber, SC, where the condensed water (stream 26) is intended to humidify the air stream feeding the cathode of the PEMFC (stream 27), to be fed to the HX unit (stream 28) and also to provide heat cogeneration (stream 29). Water circulates in an almost closed circuit, replenishing only a small aliquot which leaves the process on the off-gas streams (streams 12 and 23).

2.2 Mathematical modelling

2.2.1 Parallel plate units

The different parallel-plate reactor units proposed in the present contribution (i.e., RHX1 to RHX3) are adaptations of a design presented previously [24]. The reactor concept implies 28 sections, 3x80 mm2 each, which are separated by metallic walls (1 mm width, λ_w = 25 W/(m·K)) through which heat is transferred (see Fig. 2). For RHX1 and RHX3, alternated sections of open channels and catalytic monoliths (400 cpsi cordierite structures, 2 rows of 80 channels each) are implemented, whereas, for RHX2, catalytic monoliths are disposed in all sections. A total length of 18 cm is adopted for RHX1 and RHX2, while for RHX3 the design length is of 6 cm.

In RHX1 the thermal coupling is conducted between an inert cold stream and the catalytic combustion of the retentate stream (plus extra ethanol). On the other hand, in RHX2 the catalytic combustion of hydrogen proceeds with the unused fuel from the fuel cell. As previously mentioned, a Pd/Al_2O_3 catalyst washcoated on the monolith is considered to conduct the following reactions [32–34]:

$CH_4 + 2\ O_2 \rightarrow CO_2 + 2\ H_2O$ $\quad \Delta H° = -802.3$ kJ/mol (3)

$CO + 0.5\ O_2 \rightarrow CO_2$ $\quad \Delta H° = -283.0$ kJ/mol (4)

$H_2 + 0.5\ O_2 \rightarrow H_2O$ $\quad \Delta H° = -241.8$ kJ/mol (5)

$C_2H_5OH + 0.5\ O_2 \rightarrow C_2H_4O + H_2O$ $\quad \Delta H° = -173.4$ kJ/mol (6)

$C_2H_4O + 2.5\ O_2 \rightarrow 2\ CO_2 + 2\ H_2O$ $\quad \Delta H° = -1104.3$ kJ/mol (7)

On the other hand, while reactions 3-7 take place in the hot side of RHX2, ethanol steam reforming is performed over the monoliths deposited on the cold side sections. As stated, the same catalytic system as for the combustion sections is also implemented here (Pd/Al_2O_3) [30]:

$$C_2H_5OH + H_2O \rightarrow CO_2 + CH_4 + 2\ H_2 \qquad \Delta H° = 8.3\ kJ/mol \qquad (8)$$

$$CH_4 + H_2O \leftrightarrow CO + 3\ H_2 \qquad \Delta H° = 206.1\ kJ/mol \qquad (9)$$

$$CO + H_2O \leftrightarrow CO_2 + H_2 \qquad \Delta H° = -41.2\ kJ/mol \qquad (10)$$

A one-dimensional heterogeneous model was selected to represent the behaviour of the parallel plate reactors. Steady state operation is assumed, together with the following considerations:

- Fully developed plug flow.
- Isobaric operation.
- Negligible mass and energy axial dispersion in the gas phases.
- Perfectly distributed flow in all the reactor channels. Based on this hypothesis and the assumption that all channels are exactly of the same size, it is considered that each channel behaves equal to its neighbouring channels (within the same section).
- Heat conduction through the metallic walls is considered both axially and transversely.
- The catalytic monoliths are assumed to be isothermal at each axial coordinate based on the low thickness of their walls. Axial heat conduction through the wall of the monoliths is neglected based both on their reduced thickness and the poor heat conductivity of the cordierite.
- Homogeneous reactions were neglected.

Based on the described considerations, the mathematical model which represents units with chemical reaction only in the hot side sections (hs), RHX1 and RHX3, includes the following equations. Cold side sections (cs) is considered an inert stream.

Mass balances in the gas phases

$$\dot{m}_{hs} \cdot A_{TR} \cdot \frac{dw_{i,hs}}{dz_R} = \sigma_{hs} \cdot k_{g\ i,hs} \cdot \rho_{hs} \cdot (w^c_{i,hs} - w_{i,hs}) \qquad w_{i,hs}\big|_{z_R=0} = w^0_{i,hs} \qquad (11)$$

$$\frac{dw_{i,cs}}{dz_R} = 0 \qquad w_{i,cs}\big|_{z_R=0} = w^0_{i,cs} \qquad (12)$$

where $\dot{m}$ is the specific mass flowrate of the stream, w_i and w_i^c are the mass fraction of the species *i* in the gas phase or the catalytic surface, respectively, A_{TR} is the total cross-sectional area of flow, σ is the

total perimeter of the channels in the catalytic monolith, $k_{g\,i}$ is the mass transfer coefficient for each species *i*, and ρ is the mass density of the stream.

Mass balance in the catalyst

$$k_{g\,i,hs} \cdot \rho_{hs} \cdot \left(w^{c}_{i,hs} - w_{i,hs}\right) = M_{hs} \cdot \sum_k \left(\nu_{i,k} \cdot r_k\right) \tag{13}$$

where M is the molecular weight, $\nu_{i,k}$ is the stoichiometric coefficient of each species *i* in each reaction *k*, and r_k is the reaction rate.

Energy balances in the gas phases

$$\dot{m}_{hs} \cdot A_{TR} \cdot \frac{C_{P\,hs}}{M_{hs}} \cdot \frac{dT_{hs}}{dz_R} = \sigma_{hs} \cdot h_{hs} \cdot \left(T^{c}_{hs} - T_{hs}\right) \qquad T_{hs}|_{z_R=0} = T^{0}_{hs} \tag{14}$$

$$\dot{m}_{cs} \cdot A_{TR} \cdot \frac{1}{M_{cs}} \cdot \frac{dH_{cs}}{dz_R} = \sigma_{cs} \cdot h_{cs} \cdot \left(T_w|_{x_R=L_W} - T_{cs}\right) \qquad T_{cs}|_{z_R=0} = T^{0}_{cs} \tag{15}$$

where T and T^c are the temperatures in the gas phase or the catalytic surface, respectively, H is the molar enthalpy of the stream, h is heat transfer coefficient, and C_P is the heat capacity of the stream.

Energy balance in the catalyst

$$\sigma_{hs} \cdot h_{hs} \cdot \left(T^{c}_{hs} - T_{hs}\right) + \sigma_w \cdot q_{w,hs} = -\sigma_{hs} \cdot \sum_k \left(\Delta H_k \cdot r_k\right) \tag{16}$$

where q_w is the heat transferred through the metallic walls ΔH_k is the heat of the reaction *k*.

Energy balance in the metallic wall

$$\lambda_w \cdot \left(\frac{\partial^2 T_w}{\partial x_R^2} + \frac{\partial^2 T_w}{\partial z_R^2}\right) = \frac{-q_{lost}}{A_{TW}} \qquad \begin{cases} \left.\frac{\partial T_w}{\partial z_R}\right|_{z_R=0} = \left.\frac{\partial T_w}{\partial z_R}\right|_{z=L_R} = 0 \\ T_w|_{x_R=0} = T^{c}_{hs} \\ h_{cs} \cdot \left(T_w|_{x_R=L_W} - T_{cs}\right) + q_{w,cs} = 0 \end{cases} \tag{17}$$

where λ_w is the thermal conductivity of the metallic wall and q_{lost} is the heat lost to the environment.

Heat transferred through the metallic wall

$$\begin{cases} q_{w,hs} = \lambda_w \cdot \left.\frac{\partial T_w}{\partial x_R}\right|_{x_R=0} \\ q_{w,cs} = -\lambda_w \cdot \left.\frac{\partial T_w}{\partial x_R}\right|_{x_R=L_W} \end{cases} \tag{18}$$

The equations system above is also suitable to represent the structured reforming reactor (RHX2), but here the equations concerning the gas phase balances of the cold side of the unit (eqs. 12, 15) have to be modified while including new balances for the reforming catalyst in order to include the terms related to the ethanol steam reforming reaction and the fact that these sections contain catalytic monoliths instead of open channels.

Mass balances in the gas phases

$$\dot{m}_{cs} \cdot A_{TR} \cdot \frac{dw_{i,cs}}{dz_R} = \sigma_{cs} \cdot k_{g\ i,cs} \cdot \rho_{cs} \cdot (w^c_{i,cs} - w_{i,cs}) \qquad w_{i,cs}\big|_{z_R=0} = w^0_{i,cs} \tag{19}$$

Mass balance in the catalyst

$$k_{g\ i,cs} \cdot \rho_{cs} \cdot \left(w^c_{i,cs} - w_{i,cs}\right) = M_{cs} \cdot \sum_k \left(\nu_{i,k} \cdot r_k\right) \tag{20}$$

Energy balances in the gas phases

$$\dot{m}_{cs} \cdot A_{TR} \cdot \frac{C_{P\ cs}}{M_{cs}} \cdot \frac{dT_{cs}}{dz_R} = \sigma_{cs} \cdot h_{cs} \cdot (T^c_{cs} - T_{cs}) \qquad T_{cs}|_{z_R=0} = T^0_{cs} \tag{21}$$

Energy balance in the catalyst

$$\sigma_{cs} \cdot h_{cs} \cdot (T^c_{cs} - T_{cs}) + \sigma_w \cdot q_{w,cs} = -\sigma_{cs} \cdot \sum_k (\Delta H_k \cdot r_k) \tag{22}$$

In all cases (RHX1 to RHX3), combustion reaction rates on the Pd/Al_2O_3 catalyst are evaluated according to [32] for the combustion of CH_4 and H_2, [33] for C_2H_5OH and C_2H_4O, and [34] for CO. The kinetic parameters of the rate equations 23-27 are stated in Table 1.

$$r_{hs,1} = k^0_{hs,1} \cdot \exp\left(\frac{-Ea_{hs,1}}{R \cdot T^s_{hs}}\right) \cdot p_{CH_4} \tag{23}$$

$$r_{hs,2} = k^0_{hs,2} \cdot \exp\left(\frac{-Ea_{hs,2}}{R \cdot T^s_{hs}}\right) \cdot p_{H_2} \tag{24}$$

$$r_{hs,3} = k^0_{hs,3} \cdot \exp\left(\frac{-Ea_{hs,3}}{R \cdot T^s_{hs}}\right) \cdot p_{CO} \cdot p_{O_2} \tag{25}$$

$$r_{hs,4} = k^0_{hs,4} \cdot \exp\left(\frac{-Ea_{hs,4}}{R} \cdot \left(\frac{1}{T^s_{hs}} - \frac{1}{T^{ref}_4}\right)\right) \cdot p_{C_2H_5OH} \tag{26}$$

$$r_{hs,4} = k^0_{hs,5} \cdot \exp\left(\frac{-Ea_{hs,5}}{R} \cdot \left(\frac{1}{T^s_{hs}} - \frac{1}{T^{ref}_5}\right)\right) \cdot p_{C_2H_4O} \tag{27}$$

where p_i is the partial pressure of species i ($i = CH_4, H_2, CO, O_2, C_2H_5OH, C_2H_4O$).

As presented in Figure 1, RHX1 and RHX2 are designed each with 3 fuel inlets (equally-distributed in the axial coordinate) aiming to achieve a proper distribution of the generated heat [23]. After each fuel inlet, combustion reaction rates are neglected for a length of 2 cm to represent the air/fuel mixer zone (no catalyst is deposited here). These mixers appear mandatory to provide an homogeneous distribution of the fuel in the different monolith channels downstream the mixer (see Figure 2C).

On the other hand, for RHX2, ethanol steam reforming reaction rate on the Pd/Al_2O_3 catalyst is evaluated according to [30]. The kinetic parameters of the rate equations 28-30 are stated in Table 2. Equilibrium constants, $K_{eq,2}$ and $K_{eq,3}$, were expressed and evaluated according to thermodynamics literature [35].

$$r_{cs,1} = k_1^0 \cdot \exp\left(\frac{-Ea_{cs,1}}{R \cdot T_{cs}^S}\right) \cdot \left(p_{C_2H_5OH} \cdot p_{H_2O}\right) \tag{28}$$

$$r_{cs,2} = k_2^0 \cdot \exp\left(\frac{-Ea_{cs,2}}{R \cdot T_{cs}^S}\right) \cdot \left(p_{CH_4} \cdot p_{H_2O} - \frac{p_{CO} \cdot p_{H_2}^3}{K_{eq,2}}\right) \tag{29}$$

$$r_{cs,3} = k_3^0 \cdot \exp\left(\frac{-Ea_{cs,3}}{R \cdot T_{cs}^S}\right) \cdot \left(p_{CO} \cdot p_{H_2O} - \frac{p_{CO_2} \cdot p_{H_2}}{K_{eq,3}}\right) \tag{30}$$

For the parallel-plate reactors, mass and heat transport coefficients (k_g and h, respectively) are estimated according to [36].

$$k_g = \frac{\lambda}{D} \cdot 2.978 \cdot \left(1 + 0.095 \cdot Re \cdot Sc \cdot \frac{L_X}{L_Z}\right)^{0.45} \tag{31}$$

$$h = \frac{\lambda}{L_X} \cdot 2.978 \cdot \left(1 + 0.095 \cdot Re \cdot Pr \cdot \frac{L_X}{L_Z}\right)^{0.45} \tag{32}$$

where L_X is the width of the catalytic channels in the parallel-plate reactors, and Re, Pr and Sc are the Reynolds, the Prandtl and the Schmidt numbers, respectively, for the stream inside the sections.

The HX unit follows the parallel plate concept so its associated equations are derived from the previously stated energy balances. A length of 6 cm is adopted for this unit.

Energy balances in the gas phases

$$-\dot{m}_{hs} \cdot A_{TR} \cdot \frac{C_{P\,hs}}{M_{hs}} \cdot \frac{dT_{hs}}{dz_R} = \sigma_{hs} \cdot h_{hs} \cdot \left(T_w|_{x_R=0} - T_{hs}\right) \qquad T_{hs}|_{z_R=L_R} = T_{hs}^0 \tag{33}$$

$$\dot{m}_{cs} \cdot A_{TR} \cdot \frac{C_{P\,cs}}{M_{cs}} \cdot \frac{dT_{cs}}{dz_R} = \sigma_{cs} \cdot h_{cs} \cdot \left(T_w|_{x_R=L_W} - T_{cs}\right) \qquad T_{cs}|_{z_R=0} = T_{cs}^0 \tag{34}$$

Energy balance in the metallic wall

$$\lambda_w \cdot \left(\frac{\partial^2 T_w}{\partial x_R^2} + \frac{\partial^2 T_w}{\partial z_R^2}\right) = \frac{-q_{lost}}{A_{TW}} \qquad \begin{cases} \left.\frac{\partial T_w}{\partial z_R}\right|_{z_R=0} = \left.\frac{\partial T_w}{\partial z_R}\right|_{z_R=L_R} = 0 \\ h_{hs} \cdot \left(T_w|_{x_R=0} - T_{hs}\right) + q_{w,hs} = 0 \\ h_{cs} \cdot \left(T_w|_{x_R=L_W} - T_{cs}\right) + q_{w,cs} = 0 \end{cases} \tag{35}$$

Heat transferred through the metallic wall

$$\begin{cases} q_{w,hs} = \lambda_w \cdot \left.\frac{\partial T_w}{\partial x_R}\right|_{x_R=0} \\ q_{w,cs} = -\lambda_w \cdot \left.\frac{\partial T_w}{\partial x_R}\right|_{x_R=L_W} \end{cases} \tag{36}$$

2.2.2 Membrane reactor

As mentioned before, the reformer output stream must be purified up to CO levels of less than 10 ppm to be suitable for PEMFC feeding in order to prevent poisoning of the anode catalyst thereof [37]. The purification of the hydrogen stream produced by ethanol steam reforming in the structured reactor is intended here by employing a membrane reactor (see Figure 3). The proposed membrane reactor design is an adaptation of the one presented by [38] and further information can be found in there. The equipment presents a configuration with membrane tubes inside a shell through which syngas flows. Superheated steam is used as sweep gas inside the tubes (from stream 16, see Fig. 1).

The unit consists of 61 tubes of 13.4 mm O.D. (d_{te}), 8 mm I.D. (d_{ti}) and 300 mm length, contained in a shell of 14.5 cm in internal diameter. The tubes are disposed in triangular arrangement (see Fig. 3A). The membrane tubes consist on a porous ceramic support with a dense layer of palladium deposited on the external surface (see Fig. 3B). The Fe/Cr/Cu catalyst (pellets) is packed in the shell to perform the WGS reaction (Eq. 2).

The use of steam as sweep gas, instead of N_2 as frequently proposed, seeks the straightforward separation of the permeated hydrogen by water condensation in the SC unit (see Fig. 1). With the implementation of the cooling/separation system in the SC, a significant amount of the required water for the MR can be recovered and reused in the circuit. However, the use of this sweep gas implies a large energy expenditure in terms of evaporation and overheating that could significantly reduce the efficiency of the overall process. On the other hand, a fraction of this energy can be recovered by the condensation of water (for instance, in the preheating of the humidified air to the PEMFC, see Fig. 1).

A pseudohomogeneous one-dimensional model was selected to simulate the steady-state operation of this reaction/permeation unit. Isobaric axial evolution has been considered as well. It is important to note that the model is neither isothermal nor adiabatic, which is not a common assumption in membrane reactor models. As for the rest of the units, the model considers the heat losses to the environment from the shell. In addition, the following hypotheses are considered [38]:

- The gradients of composition and temperature in the radial direction are assumed negligible based on the selection of a small diameter for the MR tubes.
- Axial and radial dispersion of mass and energy are neglected.
- Both external and internal mass transfer resistances in the catalyst pellets are neglected.
- The permeation process across the Pd layer is assumed to proceed with H_2 infinite selectivity [39].

According to the hypotheses, the mathematical model that represents the behaviour of the membrane reactor includes the following equations:

Mass balances

$$\frac{dF_{CO,ret}}{dz_R} = -A_{TM} \cdot r_{CO} \cdot \rho_B \qquad F_{CO,ret}\big|_{z_R=0} = F^0_{CO,ret} \tag{37}$$

$$\frac{dF_{H_2,ret}}{dz_R} = A_{TM} \cdot r_{CO} \cdot \rho_B - \sigma_M \cdot J_{H_2} \qquad F_{H_2,ret}\big|_{z_R=0} = F^0_{H_2,ret} \tag{38}$$

$$\frac{dF_{H_2O,per}}{dz_R} = 0 \qquad F_{H_2O,per}\big|_{z_R=0} = F^0_{H_2O,per} \tag{39}$$

$$\frac{dF_{H_2,per}}{dz_R} = \sigma_M \cdot J_{H_2} \qquad F_{H_2,per}\big|_{z_R=0} = 0 \tag{40}$$

where F_i is the molar flowrate of species *i*, J_{H_2} is the hydrogen permeation flux through the membrane and ρ_B is the catalytic packed-bed density.

Energy balances

$$F_{ret} \cdot C_{P\,ret} \cdot \frac{dT_{ret}}{dz_R} = A_{TM} \cdot r_{CO} \cdot (-\Delta H_{WGS}) \cdot \rho_B - \sigma_M \cdot U_M \cdot \left(T_{ret} - T_{per}\right) - q_{lost}$$

$$T_{ret}\big|_{z_R=0} = T^0_{ret} \tag{41}$$

$$F_{per} \cdot C_{P\,per} \cdot \frac{dT_{per}}{dz_R} = \sigma_M \cdot U_M \cdot \left(T_{ret} - T_{per}\right) + \sigma_M \cdot C_{P,H_2} \cdot \left(T_{ret} - T_{per}\right) \cdot J_{H_2}$$

$$T_{per}\big|_{z_R=0} = T^0_{per} \tag{42}$$

Permeation law

Hydrogen permeation through the Pd membrane is quantified by Sievert's law [40] (parameters from ref. [38]):

$$J_{H_2} = \frac{Q_0}{\delta_M} \cdot \exp\left(-\frac{Ea_M}{R \cdot T_{ret}}\right) \cdot \left(\sqrt{p_{H_2,ret}} - \sqrt{p_{H_2,per}}\right) \tag{43}$$

The water gas shift reaction rate (r_{CO}) is calculated by the expression proposed by [41] for a Fe/Cr/Cu catalyst.

$$r_{CO} = \frac{k}{60} \cdot \frac{K_{CO} \cdot K_{H_2O} \cdot \left(p_{CO} \cdot p_{H_2O} - \frac{p_{CO_2} \cdot p_{H_2}}{K_{eq,3}}\right)}{\left(1 + K_{CO} \cdot p_{CO} + K_{H_2O} \cdot p_{H_2O} + K_{CO_2} \cdot p_{CO_2}\right)^2} \quad (44)$$

The kinetic constant (k) and the adsorption constants (K_i) are computed according to the following equations, whose parameters are presented in Table 3:

$$k = \exp\left(-\frac{\Delta H}{R \cdot T} + \frac{\Delta S}{R}\right) \quad (45)$$

$$K_i = \exp\left(-\frac{\Delta H_i}{R \cdot T} + \frac{\Delta S_i}{R}\right) \qquad i = CO, CO_2, H_2O \quad (46)$$

In addition, global heat transfer coefficient (U_M) is adopted according to [38].

$$U_M = \frac{1}{\frac{d_{ti}}{d_{tm}} \cdot \frac{1}{h_{ret}} + r_{ti}\left(\ln\left(\frac{d_{te}}{d_{ti}}\right)/\lambda_{Al_2O_3}\right) + r_{ti}\left(\ln\left(\frac{d_{tm}}{d_{te}}\right)/\lambda_{Pd}\right) + \frac{1}{h_{per}}} \quad (47)$$

2.2.3 Separation chamber

The separation chamber (SC) is simulated considering it as a nonadiabatic vapour-liquid separator where only water is a condensable compound in the incoming hydrogen-water mixture (stream 17, permeate from the MR, and 25, cooling water from PEMFC, see Fig. 1). Therefore, the total amount of hydrogen exiting the permeate side of the membrane reactor leaves this SC unit (stream 18), while the amount of water in each outlet of the SC is a function of the pressure and temperature at which the unit is operated. The phase equilibrium of water is modelled according to Raoult's law, using Antoine's equation for the calculation of water vapour pressure. The mathematical model of the separation chamber presents terms addressing the heat transferred to preheat three streams, the air to feed the PEMFC (stream 21), the ethanol to be burned in the RHX1 and RHX2 units (stream 6), and the air for the combustion sections to be fed into RHX3 (stream 13). Additionally, a fourth coil is incorporated to recover the latent heat available in the off-gas 1 stream (stream 11). All the coils outlets were fixed at thermal equilibrium with the chamber. The mathematical model implemented to calculate the flowrates of vapor and liquid streams (18 and 26, respectively) comprises the following equations:

Mass balances

$$F^0 = F_{vap} + F_{liq} \quad (48)$$

$$\begin{cases} F^0 \cdot y^0_{H_2O} = F_{vap} \cdot y_{H_2O,vap} + F_{liq} \cdot y_{H_2O,liq} \\ y_{H_2,vap} = 1 - y_{H_2O,vap} \end{cases} \quad (49)$$

$$\begin{cases} y_{H_2O,liq} = 1 \\ y_{H_2,liq} = 0 \end{cases} \quad (50)$$

Energy balances

$$F^0 \cdot H^0 = F_{vap} \cdot H_{vap} + F_{liq} \cdot H_{liq} + Q_{SC} \quad (51)$$

$$Q_{SC} = Q_{et} + Q_{air/RHX3} + Q_{air/PEM} + Q_{offgas} \quad (52)$$

Phase equilibrium

$$y_{H_2O,vap} \cdot P = P_{H_2O}^{sat} \quad (53)$$

$$\log_{10}\left(P_{H_2O}^{sat}[bar]\right) = 5.19050 - \frac{1730.63}{T^{sat}[°C]+233.426} \quad (54)$$

where $P_{H_2O}^{sat}$ is the saturation pressure at the SC's temperature of operation, T^{sat}.

2.2.5 PEM fuel cell

The PEMFC stack mathematical model considered in this contribution is equilibrium based (isothermal and isobaric) and adopted from [42]. The power generation is calculated according to the following equations:

Unit cell voltage

Ideal unit cell voltage is computed as follows:

$$E_{rev} = E_{rev}^0 + \frac{R \cdot T_{PEM}}{2 \cdot \mathcal{F}} \cdot \left(\ln\left(\bar{p}_{H_2,an}\right) + 0.5 \cdot \ln\left(\bar{p}_{O_2,cat}\right)\right) \quad (55)$$

where $\bar{p}_{H_2,an}$ and $\bar{p}_{O_2,cat}$ are the arithmetic mean of the partial pressures of hydrogen in the anode and oxygen in the cathode, respectively. The actual cell voltage (V_{PEM}) is decreased from its equilibrium thermodynamic potential (E_{rev}) because of irreversible losses due to the current flowing. Therefore, the expression of the voltage of a single cell is given by:

$$V_{PEM} = E_{rev} - \varphi \quad (56)$$

The overpotential (φ) is fixed here to obtain a net voltage of V_{PEM} = 0.85 V.

Electrical current

The electrical current, I_{PEM}, is related to the hydrogen molar flowrate at the anode (stream 18) and its conversion therein. In this case, 80% of added hydrogen was utilized ($X_{H_2}^{PEM}$) [42], while the nonconverted H_2 is returned to be catalytically burned in RHX3 (stream 19).

$$I_{PEM} = 2 \cdot \mathcal{F} \cdot \left(F_{18} \cdot y_{H_2,18} \cdot 0.8\right) \quad (57)$$

Before entering to the PEMFC, the inlet air to the cathode (stream 23) is humidified to a relative humidity of 80%. The inlet flowrate to the cathode is calculated in order to achieve an oxygen conversion ($X_{O_2}^{PEM}$) of 50% [42].

Power generation

$$W = I_{PEM} \cdot V_{PEM} \tag{58}$$

Energy balance

To ensure a PEMFC isothermal operation, the unit must be cooled. This is fulfilled by means of a cooling water stream through a jacket. The heat to be removed (Q_{PEM}) is evaluated by means of an energy balance in the stack:

$$Q_{PEM} + W = (F_{an} \cdot H_{an} + F_{cat} \cdot H_{cat})_{in} - (F_{an} \cdot H_{an} + F_{cat} \cdot H_{cat})_{out} \tag{59}$$

$$-Q_{PEM} = F_{25} \cdot H_{25} - F_{24} \cdot H_{24} \tag{60}$$

2.3 Model implementation

The differential equations appearing in the mathematical model of each unit are discretized by means of second order central finite differences. The final system of equations is composed of a total of 104103 algebraic equations. The generated system of equations is solved with the solver BDNLSOL of gPROMS 3.6 [43]. To facilitate the resolution procedure, the units are incorporated one at a time. When the first simulation reaches the convergence a second unit is incorporated and so on. The result of its simulation is taken as a convenient starting point for the next incorporation. Once the models of all the involved units have been included, a robust initial point for the subsequent calculations is obtained, which ensures the convergence of the next simulations. Physicochemical and thermodynamic properties for the involved species and mixtures are evaluated with the software Multiflash [44], running under the gPROMS environment.

As can be seen in Fig. 1, the input streams to the process are the reactive reforming mixture (C_2H_5OH+H_2O, stream 1), the extra ethanol fuel (stream 6), the cooling water input (stream 24) and two air streams required for the catalytic combustion and for the PEMFC (streams 13 and 20, respectively). Aiming the production of 2.5 kW of electric power in the PEMFC, a solution of water and ethanol in a 6:1 molar ratio (stream 1) is fed to the system with a molar flowrate of with 155.7 mol/h, pressure of 1.13

bar and temperature of 25 °C. The extra ethanol stream, the cooling water stream and the two air inlets are fed to the process also at 1.13 bar of absolute pressure and 25 °C of temperature.

According to [30], ethanol steam reforming kinetics were fitted at temperatures up to 770 °C. This value is assumed here as the maximum allowable to both comply with the applicability range of the kinetic expression and to prevent mechanical damage in the reforming reactor materials.

Previous studies proved that the use of elevated air flowrates prevents the formation of hot spots of restrictive magnitude in the catalytic combustion side of the RHX units [23]. Therefore, the flowrate of the incoming air stream to the first combustion unit (RHX1) is fixed here to be 2.7-fold larger than the stream fed to the corresponding cold side (stream 1), being approximately 4-fold larger when considering the addition of streams 8a to 8f to the combustion side.

As stated by the mathematical model of each equipment, heat losses to the environment (q_{lost}) are included. They are quantified considering the heat flux by conduction through a layer of insulating material covering each unit in series with free convection to the atmosphere at 1 bar and 25 °C, according to procedures reported in the literature [45]. An insulation thickness of 3 cm is assumed in each unit of the process. The separation chamber and PEMFC were considered perfectly insulated to the environment (q_{lost} = 0) since those units were operated at relatively low temperatures.

2.4 System performance evaluation

The performance of the system is evaluated based on:

a) the conversions of ethanol in the reforming reactor ($X_{C_2H_5OH}^{RHX2}$), CO conversion in the membrane reactor (X_{CO}^{MR}) and the percentage of H_2 recovery in the membrane reactor (R_{H2}):

$$X_{C_2H_5OH}^{RHX2} = \frac{F_{C_2H_5OH,Stream\ 2} - F_{C_2H_5OH,Stream\ 3}}{F_{C_2H_5OH,Stream\ 2}} \cdot 100 \quad (61)$$

$$X_{CO}^{MR} = \frac{F_{CO,Stream\ 4} - F_{CO,Stream\ 5}}{F_{CO,Stream\ 4}} \cdot 100 \quad (62)$$

$$R_{H_2} = \frac{F_{H_2,Stream\ 5}}{F_{H_2,Stream\ 5} + F_{H_2,Stream\ 17}} \cdot 100 \quad (63)$$

b) the electric power generated by the PEMFC (W, see Eq. 58), the first and second-law efficiencies of the process considering W as the main energetic profit (η_1 and η_2, respectively), the first and second-law efficiencies of the process when a cogeneration heat, Q_{co}, can be obtained from stream 29 (e.g. for

facilities heating) as an additional profit ($\eta_{1,co}$ and $\eta_{2,co}$, respectively), and the potentially recoverable residual energy in the off-gas streams (streams 12 and 23) in terms of heat and exergy (Q_{off} and Ex_{off}, respectively). The exergy content of each stream ($ex_{Stream\ j}$) is evaluated as the contribution of both physical (ex^{ph}) and chemical (ex^{ch}) exergy values, according to classical thermodynamics theory [2]. The standard chemical exergy for the chemical species (ε_i) is taken from [2]. As previously mentioned, reference atmosphere conditions were supposed at 1 bar and 25 °C. The above-mentioned parameters are expressed as follows:

$$\eta_1 = \frac{W}{(F_{C_2H_5OH,Stream\ 1}+F_{C_2H_5OH,Stream\ 6})\cdot LHV_{C_2H_5OH}} \cdot 100 \quad (64)$$

$$\eta_2 = \frac{W}{(F_{C_2H_5OH,Stream\ 1}+F_{C_2H_5OH,Stream\ 6})\cdot ex_{C_2H_5OH}} \cdot 100 \quad (65)$$

$$\eta_{1,co} = \frac{W+Q_{co}}{(F_{C_2H_5OH,Stream\ 1}+F_{C_2H_5OH,Stream\ 6})\cdot LHV_{C_2H_5OH}} \cdot 100 \quad (66)$$

$$\eta_{2,co} = \frac{W+Ex(Q_{co})}{(F_{C_2H_5OH,Stream\ 1}+F_{C_2H_5OH,Stream\ 6})\cdot ex_{C_2H_5OH}} \cdot 100 \quad (67)$$

$$Q_{co} = F_{Stream\ 30} \cdot H_{Stream\ 30} - F_{Stream\ 29} \cdot H_{Stream\ 29} \quad (68)$$

$$Q_{off} = F_{Stream\ 12} \cdot \int_{T_0}^{T_{Stream\ 12}} dH_{Stream\ 12} \quad (69)$$

$$Q_{off2} = F_{Stream\ 23} \cdot \int_{T_0}^{T_{Stream\ 23}} dH_{Stream\ 23} \quad (70)$$

$$Ex_{off1} = F_{Stream\ 12} \cdot ex_{stream\ 12} \quad (71)$$

$$Ex_{off2} = F_{Stream\ 23} \cdot ex_{stream\ 23} \quad (72)$$

$$ex_{stream\ j} = \overbrace{\int_{T_0}^{T_{Stream\ j}} dH_{Stream\ j} - T_0 \cdot \int_{T_0}^{T_{Stream\ j}} dS_{Stream\ j}}^{ex^{ph}} + \overbrace{y_{i,j} \cdot \sum_i (\varepsilon_i + R \cdot T_0 \cdot \ln(y_{i,j}))}^{ex^{ch}} \quad (73)$$

3. Results and discussion

This section presents the analysis of the performance of the integrated process described above towards the production of electric power and heating. The adopted values of the variables to perform the simulations are reported in Table 4. Results in terms of molar flow, temperature and molar composition are presented in Table A1 as an appendix. The following subsection discusses the main results on the performance of the different units involved. After that, a global analysis in terms of process efficiencies and exergy destruction is addressed.

3.1 Process performance

Figures 4 to 8 show axial profiles corresponding to selected key variables in the different units of the process. Figure 4 presents the axial temperature profiles in the streams within the parallel-plate units (A: RHX1 and RHX2, B: RHX3, C: HX). Figures 5 and 6 show the product distribution in the reforming sections of RHX2 and the molar flows of the combustion fuels in RHX1 and RHX2, respectively. Regarding the operation of the membrane reactor (MR), Figure 7 exhibits axial temperature profiles and Figure 8 presents axial profiles of hydrogen molar fractions in both the retentate and permeate streams along with the evolution of the CO conversion.

According to Fig. 4, an appropriate thermal integration was achieved in the parallel-plate units. This fact can be seen in terms of the low temperature difference between the streams. Fig. 4A shows that moderated hot spots are formed at different axial positions for HRX1-3 after each fuel inlet. It is worth recalling that a 2 cm-long inert zone is implemented after each fuel inlet, which shifts the maximum temperature peaks from the injection ports to the front of the catalytic zones. The heat feedback phenomenon occurring mainly through the metallic walls attemperate the magnitude of the hot spots. The maximum temperature registered in RHX2 is 734 °C, occurring in the combustion catalytic phase at z_R = 14.4 cm. This is also the maximum temperature found in the entire process. Another fact to highlight is that the adiabatic ΔT of combustion of streams 15+8 would rise up to 1024 °C, which could be restrictive for many low-scale facilities where could be carried out in an external combustion chamber.

Considering Fig. 4B, a similar performance is observed, with very low temperature difference between the streams and a moderate hot spot produced by the hydrogen combustion implemented to help the preheating of the air stream (stream 15) before entering the RHX1. The outlet temperature of the hot side (stream 4) is now adequate for feeding the membrane reactor since is high enough as to activate the membrane permeation while avoiding the WGS catalyst sintering.

Regarding the HX unit, thermal coupling was achieved up to a lower degree. This responds to the need of operation with a higher temperature difference between the streams to enhance the driving force for heat transfer as water evaporation requires an important heat load. However, the hot side

outlet (stream 11) is found to be at only 136 °C, which indicates a satisfactory utilization of the sensible heat of the stream.

The hot spots observed in the RHX2 unit are directly influencing the evolution of the products distribution in the steam reforming process, as seen in Fig. 5. While ethanol is completely depleted in about 6 cm, methane steam reforming (Eq. 9) is clearly affected by the location of the catalytic combustion zones in the alternated sections. This fact impacts in the hydrogen production rate which clearly slows down at each non-combustion interval. Nearly all the generated methane is converted by the steam reforming reaction, with a methane split of 0.1% molar in the reformer exit (stream 3). Therefore, the hydrogen yield reaches 5.01 mol/mol$_{C2H5OH}$, reaching the value dictated by the chemical equilibrium for this system at 1.13 bar of pressure and also close to the stoichiometric maximum of 6.0 mol/mol$_{C2H5OH}$.

Fuel consumption axial profiles in HRX1 and HRX2 are shown in Fig. 6. As seen, only CO and H_2 are consumed in the first part of RHX1 (see eqs. 4 and 5, respectively) and their rate of reaction is at these conditions low enough as to achieve complete conversion just at z_R = 6 cm, where a new fuel aliquot is added. The middle portion of RHX1 presents a higher combustion rate for these non-condensable fuels and incorporates the ethanol combustion to acetaldehyde (Eq. 6) with an ethanol conversion of 94% and a much lower conversion of acetaldehyde (Eq. 7). Only after z_R = 12 cm (the third part of the reactor RHX1+RHX2), T is high enough (see Figura 4A) as to activate methane conversion (Eq. 3). However, as observed from Fig. 6, it is important to emphasize that the methane flowrate is significantly lower than those of the other fuels (see Table A1, stream 8). On the other hand, in the case of RHX2, although temperature is higher and fuels conversions are almost instantaneous, the reaction rates are not much higher than in RHX1. This effect is due to the limitations imposed here by the species mass transfer between the gas phase and the catalytic surfaces. After exiting both RHX1 and RHX2, complete conversion of all fuels is achieved, which is a desirable condition in order to maximize the energetic utilization of the combustion stream.

Regarding the membrane reactor, Fig. 7 exhibits axial temperature profiles of both retentate and permeate streams. As seen, thermal coupling between the streams is achieved after z_R = 7 cm. However, a slight decoupling towards the reactor end is appreciated (~2 °C). This minimum effect obeys to the fact that the heat provided by the permeate stream (hot stream) does not compensate the heat lost to the environment, since the MR unit possesses a high external area and sufficiently high temperature.

Axial products distribution in the membrane reactor is shown in Fig. 8 in terms of CO conversion and hydrogen molar fraction at both sides of the membrane. As it can be seen, CO conversion shows a steep increase at the reactor inlet and, then on, it keeps an almost constant slope. This behaviour responds to a fast approach to the equilibrium achieved by an appropriate WGS catalyst at high temperature followed by the continuous shift of the chemical equilibrium towards the products (see Eq. 2) due to the hydrogen permeation through the membrane. This permeation phenomenon influences the hydrogen molar fraction profiles. In fact, the hydrogen molar fraction corresponding to the retentate stream increases in the very first region due to the WGS reaction but then drops due to the permeation with the consequent increase in the permeate side. At the reactor outlet coordinate, hydrogen permeation is still active since a driving force is still observable ($p_{H2,per} < p_{H2,ret}$).

3.2 Global thermal integration

An analysis concerning global energy and exergy balances for the proposed process is presented in this section; main results are summarized in Figures 9 and 10. Fig. 9 presents Sankey diagrams in which the final use of the invested calorific power of the streams is detailed. On the other hand, Fig. 10 shows a pie diagram addressing the distribution of the total exergy destruction in the different units involved in the process.

As presented in Fig. 9A, the total energy income to the process is given by the heating value of the ethanol in feed, which is composed by two streams: stream 1, process ethanol (fed together with water) towards ethanol steam reforming, and stream 6, as combustion feedstock in units RHX1 and RHX2. The first inlet, in stream 1, is the one with the highest value since it is aimed to produce the main hydrogen stream to feed the PEM fuel cell after its purification. On the other hand, the stream 6 is intended to

provide the heat necessary to control the outlet temperature of RHX2 at 730 °C. Depending on the global performance of the different units in the process, the distribution between the streams 1 and 6 may vary according to the need to produce more hydrogen or to have a higher heating value in the combustion sections. For instance, if the hydrogen recovery in the membrane reactor fell, the hydrogen flowrate to the PEMFC would decrease and more flowrate of the stream 1 would be necessary to recover the production of 2.5 kW. However, this reduction in the permeation flux of the MR would allow more hydrogen as fuel for the combustion channels, reducing the requirement of ethanol extra in stream 6. In this way, the relation F_1/F_6 would increase. In both cases, W_{PEM} would remain at 2.5 kW, with low modifications in thermal efficiencies. Table 5 sums up the main results addressing the performance of the process, according to the operative conditions already stated in Tables 4 and 5.

Among the results presented in Table 5, some points are worth remarking. Firstly, process ethanol conversion in the RHX2 is 100%, which is essential to achieve optimal hydrogen yields. In addition, the CO conversion in the MR is 63.8%, which is far superior from that which could be achieved in a conventional WGS packed bed reactor at 541 °C (considering a CO inlet of more than 8%, see Table A1). Hydrogen recovery in the membrane reactor is 54.5%. This value appears perfectible since, as presented in Fig. 8, the driving force for the permeation process is not totally extinct at the end of the reactor, avoiding some extra hydrogen extraction towards the PEMFC (or using a lean process ethanol mixture). However, and despite this medium H_2 recovery value, it should be emphasized that the hydrogen purification method adopted (i.e., use of a MR with sweep gas) allows the complete process operation at a pressure level very close to the atmospheric and, in these terms, minimal work of compression/pumping is required. This fact not only impacts on the overall energy balance, but simplifies as well the process layout in this medium/small scale facility. Moreover, it is worth remarking that all non-permeated hydrogen remains in the system (i.e., is not vented) and it is entirely profited as fuel in the combustion channels of RHX1 and RHX2, consequently diminishing the need of extra ethanol for heating the reactors.

Table 6 reports thermal efficiencies (without and with cogeneration, η_1 and $\eta_{1,co}$, respectively) for different power production processes among the literature, which are based exclusively on ethanol reforming. We decided here to make focus only on ER processes to limit the extent of the available data and to compare performances on a common basis. As seen in Table 6, the operating conditions of the processes under comparison show a wide variability, from atmospheric to medium pressures, different steam-to-carbon ratios and from 500 to 700°C, aproximately. Additionally, electric powers ranging from 15 W to 500 kW are included. Among the remarkable variability in operating conditions and production scale under simulation depicted in Table 6, our process compares accordingly with the performances reported by other authors. Specifically, the process presented by this contribution shows a thermal efficiency, η_1, of 25.3% which is not far from those reported in literature for processes operating at higher pressures (which would allow higher permeation fluxes) or lower steam-to-ethanol ratios (which reduces the energy requirements for extra water evaporation). Moreover, the thermal efficiency considering heat cogeneration, $\eta_{1,co}$, reaches up to 56.3%, an improved result that not only provides an electric power of 2.5 kW, but also leaves available a source of heat of 3.06 kW (Fig. 9A) which appears appealing if the process is thought to provide both electric power and heating (e.g., for a small house or facility).

Figure 9B reports the global exergy balance for the studied process. In this case, the global balance shows that the exergy income to the process is close to the energy income since the definition of the chemical exergy of fuels is directly related to their heating value [2]. Then, as stated in Table 5, the exergetic efficiency of the process, η_2, is 23.3%. However, the exergetic efficiency with heat cogeneration, $\eta_{2,co}$, diverges from $\eta_{1,co}$, since the cogeneration heat, Q_{co} (the term which allows the efficiencies augment), is 100% energetic but it is not fully convertible to power, so its associated exergy, Ex_{co}, is diminished by its irreversible character and $\eta_{2,co}$ is 32.1%.

As Fig. 9B shows that the main source of exergetic inefficiency is not the heat released with the off-gas streams but the exergy destruction, which accumulates 6.79 kW in the whole process. The different sources of exergy destruction and their contribution to the total quantity are shown in Figure 10.

The distribution of exergy destruction presented by Fig. 10 shows a strong contribution of the process reactors, with RHX1 and RHX2 together summing more than a half of the total (52.4%). In addition, RHX3 contributes with a 9.4% and the fuel cell, PEMFC, with a 14.2%. This fact is a consequence of the exergy loss due to the chemical reactions which proceed with a high entropy generation due to their irreversibility of these processes. This behaviour has been previously reported in systems of similar characteristics [48,51]. Moreover, HX contributes with an important fraction of the total exergy destruction as well, here based on the significant temperature difference between the streams (see Fig. 4C), which lowers the exergetic efficiency of the unit by means of a strong entropy generation associated to this thermal imbalance. This fact also proofs that, for the case of the reactors, exergy destruction would be much higher in case of implementing this process with traditional reactors in which heat transfer processes present a lower thermal efficiency due to strong thermal gradients.

Regarding the membrane reactor, is worth observing that this unit present an exergy destruction level lower than the other reactors (only 170 W), although it possesses a large volume, operates at high temperature and involves a chemical reaction. This high efficiency (i.e., low exergy destruction) results as the balance of two counteracting effects. First, the permeate stream, entering the unit at 580 °C, cools down in the reactor's tubes, losing exergetic capacity, but, simultaneously, gaining an important amount of hydrogen, a fuel with high heating value and chemical exergy. On the contrary, the retentate stream enters the MR at 490 °C and heats up in the reactor by means of the exothermic WGS reaction (Eq. 2) and the heat transferred from the sweep gas flowing along the tubes. This provokes an exergy grow that is partially attemperated by the hydrogen permeation (transferring part of its chemical exergy with it). The compensation between these effects leads to a high exergy efficiency for this unit.

4. Conclusions

In the present contribution, a highly integrated process aiming electrical and heating power supply is proposed. Ethanol, water and air at atmospheric conditions are considered as feedstocks. Main focus is put in process intensification through the use of parallel-plate and membrane reactors allowing the combination of different process operations within the units. The electric power is generated by means

of a PEM fuel cell, which is fed with pure hydrogen produced by ethanol steam reforming with subsequent purification.

According to the proposed process conditions, appropriate thermal integration is achieved both in the parallel-plate units as well as in the membrane reactor. Thanks to the metallic structure of the parallel-plate reactors and the implementation of distributed fuel injection along the axial coordinate, the magnitude of the hot spots resulting from the imbalance in the steam reforming and the combustion reaction rates could be moderated. Regarding the membrane reactor, a non-complete permeation of the available hydrogen was observed. This fact could be improved by means of augmenting the partial pressure driving force between the streams by increasing the sweep gas flowrate or by increasing the membrane area. However, the process scheme proposed here profits from the non-permeated hydrogen as fuel for the combustion section of the parallel-plate reactors. Consequently, complete H_2 abatement in the MR´s retentate would imply the need of feeding extra ethanol flowrates to be used as fuel.

In terms of global thermal integration, high reforming temperatures are needed to ensure a complete ethanol conversion and a high degree of methane reforming is also required in order to achieve the maximum hydrogen yield. The high temperature of the streams exiting the reformer allows preheating the air to the combustion sections and the sweep gas to the membrane reactor improving the process integration and achieving a thermal efficiency of 25.3%. The energetic power of the outlet permeated stream is led to a separation chamber to produce a hot water stream which is used to produce the cogeneration heat, increasing the total thermal efficiency up to 56.3%.

Declaration of interests

The authors declare that they have no known competing financial interests or personal relationships that could have appeared to influence the work reported in this paper.

5. Acknowledgements

The authors acknowledge the financial support of Consejo Nacional de Investigaciones Científicas y Técnicas (CONICET), Universidad Nacional del Sur (UNS), and Agencia Nacional de Promoción Científica y Tecnológica (ANPCyT).

References

[1] K. Sundmacher, A. Kienle, A. Seidel-Morgenstern, Integrated Chemical Processes. Synthesis, Operation, Analysis, and Control, Wiley-VCH, Weinheim, Germany, 2005.

[2] M.J. Moran, H.N. Shapiro, D.D. Boettner, M.B. Bailet, Fundamentals of Engineering Thermodynamics, 7th ed., John Wiley & Sons, Hoboken, NJ, 2010.

[3] A.C. Dimian, Integrated Design and Simulation of Chemical Processes, Elsevier, Amsterdam, 2003.

[4] D. Reay, C. Ramshaw, A. Harvey, Process Intensification. Engineering for Efficiency, Sustainability and Flexibility, Elsevier, Amsterdam, 2008.

[5] M. Baldea, From process integration to process intensification, Comput. Chem. Eng. 81 (2015) 104–114. doi:10.1016/j.compchemeng.2015.03.011.

[6] R.P. Utikar, V. V. Ranade, Intensifying multiphase reactions and reactors. Strategies and examples, ACS Sustain. Chem. Eng. 5 (2017) 3607–3622. doi:10.1021/acssuschemeng.6b03017.

[7] R.E. Hayes, S.T. Kolaczkowski, Introduction to catalytic combustion, Gordon and Breach Science Publishers, Amsterdam, 1998.

[8] C.H. Phillips, G. Lauschke, H. Peerhossaini, Intensification of batch chemical processes by using integrated chemical reactor-heat exchangers, Appl. Therm. Eng. 17 (1997) 809–824. doi:10.1016/S1359-4311(96)00061-0.

[9] M. Cabassud, C. Gourdon, Intensification of heat transfer in chemical reactors: Heat exchanger reactors, in: A. Cybulski, J.A. Moulijn (Eds.), Nov. Concepts Catal. Chem. React. Improv. Effic. Futur., Wiley-VCH, Weinheim, Germany, 2010: pp. 261–287. doi:10.1002/9783527630882.ch12.

[10] J. Frauhammer, G. Eigenberger, L. V. Hippel, D. Arntz, A new reactor concept for endothermic high-temperature reactions, Chem. Eng. Sci. 54 (1999) 3661–3670. doi:10.1016/S0009-2509(98)00454-0.

[11] G. Kolios, J. Frauhammer, G. Eigenberger, Efficient reactor concepts for coupling of endothermic and exothermic reactions, Chem. Eng. Sci. 57 (2002) 1505–1510. doi:10.1016/S0009-2509(02)00022-2.

[12] G. Kolios, A. Gritsch, A. Morillo, U. Tuttlies, J. Bernnat, F. Opferkuch, G. Eigenberger, Heat-integrated reactor concepts for catalytic reforming and automotive exhaust purification, Appl.

Catal. B Environ. 70 (2007) 16–30. doi:10.1016/j.apcatb.2006.01.030.

[13] M.E. Adrover, E. López, D.O. Borio, M.N. Pedernera, Heat effects in a membrane reactor for the water gas shift reaction, Nat. Gas Convers. VIII. (2007) 183–188.

[14] C.A. Cornaglia, M.E. Adrover, J.F. Múnera Agudelo, M.N. Pedernera, D.O. Borio, E.A. Lombardo, Production of ultrapure hydrogen in a Pd-Ag membrane reactor using noble metals supported on La-Si oxides. Heterogeneous modeling for the water gas shift reaction, Int. J. Hydrogen Energy. 38 (2013) 10485–10493. doi:10.1016/j.ijhydene.2013.05.043.

[15] M.L. Rodríguez, D.E. Ardissone, E. López, M.N. Pedernera, D.O. Borio, Reactor designs for ethylene production via ethane oxidative dehydrogenation: Comparison of performance, Ind. Eng. Chem. Res. 50 (2011) 2690–2697. doi:10.1021/ie100738q.

[16] M.L. Rodríguez, M.N. Pedernera, D.O. Borio, Two dimensional modeling of a membrane reactor for ATR of methane, Catal. Today. 193 (2012) 137–144. doi:10.1016/j.cattod.2012.04.010.

[17] U. Gardemann, M. Steffen, A. Heinzel, Design and demonstration of an ethanol fuel processor for HT-PEM fuel cell applications, Int. J. Hydrogen Energy. 39 (2014) 18135–18145. doi:10.1016/j.ijhydene.2014.05.027.

[18] L. Hernández, V. Kafarov, Use of bioethanol for sustainable electrical energy production, Int. J. Hydrogen Energy. 34 (2009) 7041–4050. doi:10.1016/j.ijhydene.2008.07.089.

[19] H. Zabed, J.N. Sahu, A. Suely, A.N. Boyce, G. Faruq, Bioethanol production from renewable sources: Current perspectives and technological progress, Renew. Sustain. Energy Rev. 71 (2017) 475–501. doi:10.1016/j.rser.2016.12.076.

[20] P.D. Vaidya, A.E. Rodrigues, Insight into steam reforming of ethanol to produce hydrogen for fuel cells, Chem. Eng. J. 117 (2006) 39–49. doi:10.1016/j.cej.2005.12.008.

[21] G. Manzolini, S. Tosti, Hydrogen production from ethanol steam reforming: energy efficiency analysis of traditional and membrane processes, Int. J. Hydrogen Energy. 33 (2008) 5571–5582. doi:10.1016/j.ijhydene.2008.06.029.

[22] J.L. Contreras, J. Salmones, J.A. Colín-Luna, L. Nuño, B. Quintana, I. Córdova, B. Zeifert, C. Tapia, G.A. Fuentes, Catalysts for H2 production using the ethanol steam reforming (a review), Int. J. Hydrogen Energy. 39 (2014) 18835–18853. doi:10.1016/j.ijhydene.2014.08.072.

[23] E.M. Izurieta, D.O. Borio, M.N. Pedernera, E. López, Parallel plates reactor simulation: Ethanol steam reforming thermally coupled with ethanol combustion, Int. J. Hydrogen Energy. 42 (2017) 18794–18804. doi:10.1016/j.ijhydene.2017.06.134.

[24] E.M. Izurieta, M.N. Pedernera, E. López, Study of a thermally integrated parallel plates reactor for hydrogen production, Chem. Eng. Sci. 196 (2019) 344–353. doi:10.1016/j.ces.2018.11.011.

[25] J.A. Torres Rivero, Catalysts for steam reforming of ethanol in a catalytic wall reactor, Ph.D. Thesis (Universitat Rovira i Virgili, Spain), Tarragona, 2007. http://hdl.handle.net/10803/8565.

[26] R. Nedyalkova, A. Casanovas, J. Llorca Piqué, D. Montané, Electrophoretic deposition of Co-Me/ZnO (Me = Mn,Fe) ethanol steam reforming catalysts on stainless steel plates, Int. J. Hydrogen Energy. 34 (2009) 2591–2599. doi:10.1016/j.ijhydene.2009.01.050.

[27] C. Cao, Y. Wang, R.T. Rozmiarek, Heterogeneous reactor model for steam reforming of methane in a microchannel reactor with microstructured catalysts, Catal. Today. 110 (2005) 92–97. doi:10.1016/j.cattod.2005.09.004.

[28] V. Palma, M. Martino, E. Meloni, A. Ricca, Novel structured catalysts configuration for intensification of steam reforming of methane, Int. J. Hydrogen Energy. 42 (2017) 1629–1638. doi:10.1016/j.ijhydene.2016.06.162.

[29] M.E. Adrover, D.O. Borio, M.N. Pedernera, Comparison between WGS membrane reactors operating with and without sweep gas: Limiting conditions for co-current flow, Int. J. Hydrogen Energy. 42 (2017) 5139–5149. doi:10.1016/j.ijhydene.2016.11.075.

[30] E. López, V. Gepert, A. Gritsch, U. Nieken, G. Eigenberger, Ethanol steam reforming thermally coupled with fuel combustion in a parallel plate reactor, Ind. Eng. Chem. Res. 51 (2012) 4143–4151. doi:10.1021/ie202364y.

[31] Y.M. Bruschi, E. López, M.N. Pedernera, D.O. Borio, Coupling exothermic and endothermic reactions in an ethanol microreformer for H2 production, Chem. Eng. J. 294 (2016) 97–104. doi:10.1016/j.cej.2016.02.079.

[32] A. Gritsch, Wärmeintegrierte Reaktorkonzepte für katalytische Hochtemperatur-Synthesen am Beispiel der dezentralen Dampfreformierung von Methan, Ph.D. Thesis (Universität Stuttgart, Germany), Sttutgart, 2008. http://elib.uni-stuttgart.de/handle/11682/1788.

[33] Y.M. Bruschi, Estudio de micro-reactores para la generación de gas de síntesis, Ph.D. Thesis (Universidad Nacional del Sur, Argentina), Bahía Blanca, 2014. http://repositoriodigital.uns.edu.ar/handle/123456789/437.

[34] K. Daneshvar, R. Krishna Dadi, D. Luss, V. Balakotaiah, S.B. Kang, C.M. Kalamaras, W.S. Epling, Experimental and modeling study of CO and hydrocarbons light-off on various Pt-Pd/Al2O3 diesel oxidation catalysts, Chem. Eng. J. 323 (2017) 347–360. doi:10.1016/j.cej.2017.04.078.

[35] J.R. Elliott, C.T. Lira, Introductory Chemical Engineering Thermodynamics, 2nd ed., Prentice Hall, 2012.

[36] A. Cybulski, J.A. Moulijn, Monoliths in Heterogeneous Catalysis, Catal. Rev. Sci. Eng. 36 (1994) 179–270. doi:10.1080/01614949408013925.

[37] C. Song, Fuel processing for low-temperature and high-temperature fuel cells. Challenges, and opportunities for sustainable development in the 21st century, Catal. Today. 77 (2002) 17–49.

[38] M.E. Adrover, E. López, D.O. Borio, M.N. Pedernera, Simulation of a membrane reactor for the WGS reaction: Pressure and thermal effects, Chem. Eng. J. 154 (2009) 196–202. doi:10.1016/j.cej.2009.04.057.

[39] D. Edlund, Hydrogen membrane technologies and application in fuel processing, in: K. Liu, C. Song, V. Subramani (Eds.), Hydrog. Syngas Prod. Purif. Technol., John Wiley & Sons, Hoboken, NJ, 2010.

[40] G. Barbieri, A. Brunetti, T. Granato, P. Bernardo, E. Drioli, Engineering evaluations of a catalytic membrane reactor for the water gas shift reaction, Ind. Eng. Chem. Res. 44 (2005) 7676–7683. doi:Doi 10.1021/Ie050357h.

[41] W.F. Podolski, Y.G. Kim, Modeling the water-gas shift reaction, Ind. Eng. Chem. Process Des. Dev. 13 (1974) 415–421. doi:10.1021/i260052a021.

[42] J.A. Francesconi, M.C. Mussati, R.O. Mato, P.A. Aguirre, Analysis of the energy efficiency of an integrated ethanol processor for PEM fuel cell systems, J. Power Sources. 167 (2007) 151–161. doi:10.1016/j.jpowsour.2006.12.109.

[43] PSE, gPROMS Advanced User Guide, Process Systems Enterprise Ltd., London, 2004.

[44] ICS, User Guide for Multiflash Models and Physical Properties, Infochem Computer Services Ltd.,

London, 2012.

[45] T.L. Bergman, A.S. Lavine, F.P. Incropera, D.P. Dewitt, Fundamentals of heat and mass transfer, John Wiley & Sons, 2011.

[46] J.A. Francesconi, M.C. Mussati, P.A. Aguirre, Effects of PEMFC operating parameters on the performance of an integrated ethanol processor, Int. J. Hydrogen Energy. 35 (2010) 5940–5946. doi:10.1016/j.ijhydene.2009.12.103.

[47] J.L. Viviente, J. Meléndez, D.A. Pacheco Tanaka, F. Gallucci, V. Spallina, G. Manzolini, S. Foresti, V. Palma, C. Ruocco, L. Roses, Advanced m-CHP fuel cell system based on a novel bio-ethanol fluidized bed membrane reformer, Int. J. Hydrogen Energy. 42 (2017) 13970–13987. doi:10.1016/j.ijhydene.2017.03.162.

[48] Y. Casas, L.E. Arteaga, M. Morales, E. Rosa, L.M. Peralta, J. Dewulf, Energy and exergy analysis of an ethanol fueled solid oxide fuel cell power plant, Chem. Eng. J. 162 (2010) 1057–1066. doi:10.1016/j.cej.2010.06.021.

[49] A. Hedayati, O. Le Corre, B. Lacarrière, J. Llorca, Exergetic study of catalytic steam reforming of bio-ethanol over Pd-Rh/CeO2 with hydrogen purification in a membrane reactor, Int. J. Hydrogen Energy. 40 (2015) 3574–3581. doi:10.1016/j.ijhydene.2014.09.016.

[50] E.M. Izurieta, M.E. Adrover, M.N. Pedernera, E. López, Ethanol processor design for hydrogen production. Kinetic analysis and process integration, Ind. Eng. Chem. Res. (2018). doi:10.1021/acs.iecr.8b02324.

[51] A.P. Simpson, A.E. Lutz, Exergy analysis of hydrogen production via steam methane reforming, Int. J. Hydrogen Energy. 32 (2007) 4811–4820. doi:10.1016/j.ijhydene.2007.08.025.

Figure 1. Process flow diagram.

Figure 2. A) Parallel plate reactor to integrate reaction and heat exchange (RHX). B) Detail on the monolith channels for RHX2. C) Upper view of a combustion section. Detail on fuel/air mixing zone.

Figure 3. A) Membrane reactor (MR). B) Detail on a membrane tube.

Figure 4. Axial temperature profiles for the parallel-plate units. A) RHX1 and RHX2. B) RHX3. C) HX. Inlet and outlet streams' numbers are indicated by circled labels (see Fig. 1).

Figure 5. Axial species distribution in the reforming sections of RHX2, in terms of molar yield (mol of species per mol of fed ethanol to this reactor).

Figure 6. Axial molar flowrate distribution for the different fuels in the combustion sections of RHX1 and RHX2.

Figure 7. Axial temperature distribution in the membrane reactor.

Figure 8. Axial profiles of CO conversion and H_2 molar fraction both in the retentate and the permeate streams for the membrane reactor.

Figure 9. Sankey diagrams for the global energy (A) and exergy (B) balances of the process.

Figure 10. Percentual distribution of the total exergy destruction in the different units of the process.

Table 1. Kinetic parameters for the rate equations representing catalytic combustion (Eqs. 23 to 27).

Reaction	k^0	Ea	T^{ref}
1 (Eq. 23) [32]	20000 mol/m^2·s·bar	74000 J/mol	
2 (Eq. 24) [32]	130000 mol/m^2·s·bar	41570 J/mol	
3 (Eq. 25) [34]	3437500 mol/m^2·s·bar^2	70000 J/mol	
4 (Eq. 26) [33]	0.661 mol/m^2·s·bar	169100 J/mol	598 K
5 (Eq. 27) [33]	1.233 mol/m^2·s·bar	135900 J/mol	723 K

Table 2. Kinetic parameters for the rate equations representing ethanol steam reforming (Eqs. 28 to 30).

Reaction	k^0	Ea
1 (Eq. 28)	$9.40 \cdot 10^5$ kmol/m^2·s·bar^n	148000 J/mol
2 (Eq. 29)	$8.22 \cdot 10^2$ kmol/m^2·s·bar^n	107300 J/mol
3 (Eq. 30)	$3.01 \cdot 10^{-1}$ kmol/m^2·s·bar^n	59900 J/mol

Table 3. Kinetic parameters for the rate equation of water-gas shift reaction (Eqs. 43 and 44).

	ΔH [cal/mol]	ΔS [cal/mol·K]
k [mol/g·min]	29364	40.32
K_{CO} [bar^{-1}]	-3064	-6.74
K_{H_2O} [bar^{-1}]	-12542	-18.45
K_{CO_2} [bar^{-1}]	6216	12.77

Table 4. Fixed variables for the studied process.

W_{PEM}	2.50 kW	$X_{H_2}^{PEM}$	80%
V_{PEM}	0.85 V	$X_{O_2}^{PEM}$	50%
H_2 humidity to PEMFC	100%	T_3	730 °C
O_2 humidity to PEMFC	80%	F_4/F_{16}	1.25
T_{PEM}	80 °C	F_{15}/F_1	2.7

Table 5. Indicators of the performance for the process (see Eqs. 59 to 70).

$X_{C_2H_5OH}^{RHX2}$	100%	R_{H_2}	54.5%
X_{CO}^{MR}	63.8%	Q_{co}	3.06 kW
η_1	25.3%	Q_{off1}	2.05 kW
$\eta_{1,co}$	56.3%	Q_{off2}	1.96 kW
η_2	23.3%	Ex_{off1}	0.22 kW
$\eta_{2,co}$	32.1%	Ex_{off2}	0.17 kW

Table 6. Comparison of thermal efficiencies from different ethanol processors for hydrogen production.

	Steam-to-carbon ratio	P [bar]	$T_{reforming}$ [°C]	W [kW]	η_1 [%]	$\eta_{1,co}$ [%]
This work	3.0	1.13	705	2.5	25.3	56.3
Francesconi et al. [46][a]	2.0	2.00	709	3.0	28.8	
Viviente et al. [47][a]	3.0	2.00	600	5.0	33.1	57.1
Viviente et al. [47][b]	2.2	12.0	500	5.0	39.3	48.9
Casas et al. [48][c]	3.0	1.00	650	500	37.6	
Hedayati et al. [49][d]	1.6	12.0	650	0.015	20.0	
Izurieta et al. [50][d]	3.0	1.13	550	0.5	23.7	

[a] H_2 purification is achieved using WGS and CO-Prox packed-bed reactors.

[b] Authothermal ethanol reforming in a membrane reactor.

[c] Power generation is made in a Solid Oxide Fuel Cell (SOFC).

[d] Electric power supply is calculated according to the reported data and assuming a $X_{H_2}^{PEM}$ = 75%. The referred papers only consider the production and purification of H_2 (A fuel cell is not proposed).

Appendix: Process simulation results

The Table A1 in this appendix presents the main results of the process simulation.

Stream	**1**	**2**	**3**	**4**	**5**	**6**	**7**	**8**	**9**	**10**
F [mol/h]	157.1	157.1	246.3	246.3	177.7	5.4	5.4	183.1	502.9	580.9
T [°C]	25.0	535.7	730.0	490.3	541.1	25.0	80.0	506.5	536.0	730.2
y_{C2H5OH} [%]	14.29	14.29	0.00	0.00	0.00	100.00	100.00	2.95	0.00	0.00
y_{H2O} [%]	85.71	85.71	36.18	36.18	42.49	0.00	0.00	41.24	19.50	29.77
y_{H2} [%]	0.00	0.00	45.60	45.60	32.26	0.00	0.00	31.30	0.00	0.00
y_{CO2} [%]	0.00	0.00	9.47	9.47	20.77	0.00	0.00	20.16	5.53	9.59
y_{CH4} [%]	0.00	0.00	0.10	0.10	0.14	0.00	0.00	0.14	0.01	0.00
y_{CO} [%]	0.00	0.00	8.64	8.64	4.33	0.00	0.00	4.21	0.00	0.00
y_{O2} [%]	0.00	0.00	0.00	0.00	0.00	0.00	0.00	0.00	10.81	5.11
y_{N2} [%]	0.00	0.00	0.00	0.00	0.00	0.00	0.00	0.00	64.15	55.54
Stream	**11**	**12**	**13**	**14**	**15**	**16**	**17**	**18**	**19**	**20**
F [mol/h]	580.9	580.9	408.4	408.4	424.9	197.0	265.6	116.8	23.4	261.3
T [°C]	136.0	80.0	25.0	80.0	490.4	580.0	542.9	80.0	80.0	25.0
y_{C2H5OH} [%]	0.00	0.00	0.00	0.00	0.00	0.00	0.00	0.00	0.00	0.00
y_{H2O} [%]	29.77	29.77	0.00	0.00	5.50	100.00	74.18	41.28	41.28	0.00
y_{H2} [%]	0.00	0.00	0.00	0.00	0.00	0.00	25.82	58.72	58.72	0.00
y_{CO2} [%]	9.59	9.59	0.00	0.00	0.00	0.00	0.00	0.00	0.00	0.00
y_{CH4} [%]	0.00	0.00	0.00	0.00	0.00	0.00	0.00	0.00	0.00	0.00
y_{CO} [%]	0.00	0.00	0.00	0.00	0.00	0.00	0.00	0.00	0.00	0.00
y_{O2} [%]	5.11	5.11	21.00	21.00	18.57	0.00	0.00	0.00	0.00	21.00
y_{N2} [%]	55.54	55.54	79.00	79.00	75.93	0.00	0.00	0.00	0.00	79.00
Stream	21	22	23	24	25	26	27	28	29	30

F [mol/h]	390.1	390.1	398.3	2778.5	2836.4	2985.2	128.8	197.0	2659.3	2659.3
T [°C]	30.2	80.0	80.0	25.0	57.6	80.0	80.0	80.0	80.0	25.0
y_{C2H5OH} [%]	0.00	0.00	0.00	0.00	0.00	0.00	0.00	0.00	0.00	0.00
y_{H2O} [%]	33.03	33.03	41.28	100.00	100.00	100.00	100.00	100.00	100.00	100.00
y_{H2} [%]	0.00	0.00	0.00	0.00	0.00	0.00	0.00	0.00	0.00	0.00
y_{CO2} [%]	0.00	0.00	0.00	0.00	0.00	0.00	0.00	0.00	0.00	0.00
y_{CH4} [%]	0.00	0.00	0.00	0.00	0.00	0.00	0.00	0.00	0.00	0.00
y_{CO} [%]	0.00	0.00	0.00	0.00	0.00	0.00	0.00	0.00	0.00	0.00
y_{O2} [%]	14.06	14.06	6.89	0.00	0.00	0.00	0.00	0.00	0.00	0.00
y_{N2} [%]	52.91	52.91	51.83	0.00	0.00	0.00	0.00	0.00	0.00	0.00
Stream 9 presents the higher concentration of acetaldehyde, $y_{C2H4O} = 1.3 \cdot 10^{-5}$ % molar. The complete process is considered isobaric at 1.13 bar.										

Table A1. Operative conditions for each stream in the process (see Fig. 1 for stream nomenclature).